The SuperMAG data processing technique

J. W. Gjerloev[1,2]

Received 2 March 2012; revised 24 July 2012; accepted 24 July 2012; published 14 September 2012.

[1] In this paper I outline the data processing technique which is used in the SuperMAG initiative. SuperMAG is a worldwide collaboration of organizations and national agencies that currently operate more than 300 ground based magnetometers. SuperMAG provides easy access to validated ground magnetic field perturbations in the same coordinate system, identical time resolution and with a common baseline removal approach. The purpose of SuperMAG is to provide scientists, teachers, students and the general public easy access to measurements of the magnetic field at the surface of the Earth. Easy access to data, plots and derived products maximizes the utilization of this unique data set. It is outlined how SuperMAG processes the observations obtained by the individual data provider. Data are rotated into a local magnetic coordinate system by determining a time dependent declination angle. This angle displays a slow gradual change and a yearly periodic variation attributed to changes in the Earth main field and season temperature variations. The baseline is determined from the data itself in a three step process: (1) a daily baseline, (2) a yearly trend, and (3) a residual offset. This technique does not require so-called quiet days and thus it avoids all the well-known problems associated with their identification. The residual offset for the N- and Z-components shows a distinct latitudinal dependence while the E-component is independent of the latitude. This result is interpreted as being due to a weak ring current (likely asymmetric) which is present even during official quiet days. For the purpose of M-I research using 1-min data I find no difference between observatories and variometers. I finally argue that there is no correct baseline determination technique since we do not have a set of ground-truth observations required to make an objective evaluation. Instead, the user must keep in mind the assumptions on which the baseline was determined and draw conclusions accordingly.

Citation: Gjerloev, J. W. (2012), The SuperMAG data processing technique, *J. Geophys. Res.*, *117*, A09213, doi:10.1029/2012JA017683.

1. Introduction

[2] For decades ground based magnetometers have been the workhorse of magnetosphere-ionosphere (M-I) physics and their importance is indisputable. Popular indices such as Kp, AE and Dst are all derived from ground based magnetometer measurements and within the last two decades the use of ground magnetometer observations from sites worldwide has found application in estimating global scale electrodynamics by means of assimilation techniques [e.g., *Richmond and Kamide*, 1988; *Lu et al.*, 1996]. Magnetometers have played a central role in a long list of published studies, for example: The structure and behavior of the auroral electrojets system (e.g., DP2 current system [*Nishida*, 1971; *Gjerloev et al.*, 2010]; substorm growth phase [*McPherron*, 1970]; two-component electrojets system [*Kamide and Kokubun*, 1996]); traveling convection vortices [*Lanzerotti et al.*, 1986; *Friis-Christensen et al.*, 1988; *Glassmeier et al.*, 1989]; characteristic response time of the magnetosphere-ionosphere system to relatively discontinuous changes in the IMF [e.g., *Murr and Hughes*, 2001]; long-term behavior of the current systems [e.g., *Kihn and Ridley*, 2005; *Ridley and Kihn*, 2004]; and ULF waves [e.g., *Anderson et al.*, 1990; *Takahashi and Anderson*, 1992; *Elkington et al.*, 1999]. The list of discoveries and other scientific advances for which ground based magnetometer data played a key role is very extensive. The above short list of publications and topics is by no means intended to be complete but is simply included to illustrate the historic success of magnetometers and the fact that they continue to serve as an indispensable measurement.

[3] Advancing our understanding of the system dynamics and structure hinges on global and continuous data coverage. Including data obtained by many different providers comes with considerable challenges of different nature: practical, computational and physics. Combining all stations into a global continuous monitoring system was therefore the next logical step for the ground magnetometer community.

[1]Department of Physics and Technology, University of Bergen, Bergen, Norway.
[2]Johns Hopkins University Applied Physics Laboratory, Laurel, Maryland, USA.

Corresponding author: J. W. Gjerloev, Department of Physics and Technology, University of Bergen, Allegt. 55, Bergen NO-5007, Norway. (jesper.gjerloev@ift.uib.no)

0148-0227/12/2012JA017683

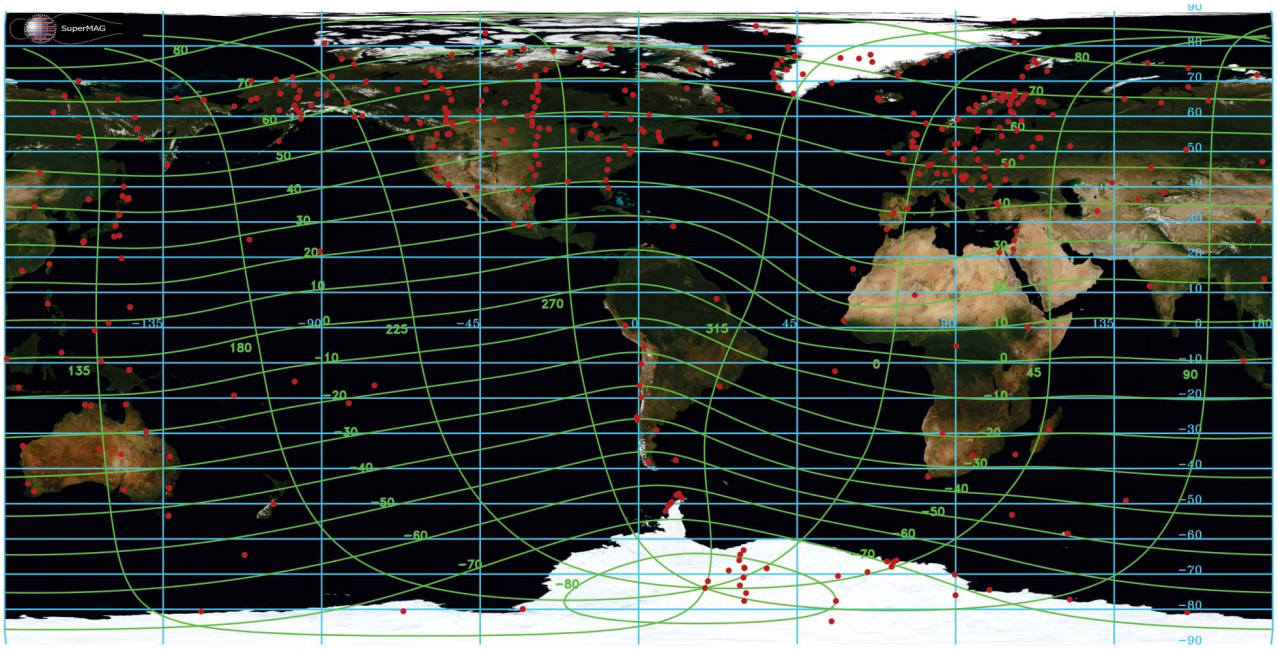

Figure 1. Location of the world's ground based magnetometers (red dots) in geomagnetic coordinates (cyan coordinates) and with geographic coordinates superposed (green). Notice the vast number of stations providing a powerful data set for global and continuous monitoring of the ground magnetic field. The map is approximate as some stations may be out of service.

[4] SuperMAG [*Gjerloev*, 2009] (http://supermag.uib.no and http://supermag.jhuapl.edu) is a worldwide collaboration of organizations and national agencies which currently operate more than 300 ground-based magnetometers spread across the globe (see Figure 1). As of July 2012, the members of the SuperMAG family are Intermagnet, Penguin, Greenland, Izmiran, Carisma, Kyoto WDC, Image, Autumn, SAMBA, ICESTAR, SAMNET, Athabasca U., MEASURE, BAS, MACCS, RapidMAG, 210 Chain, BGS, AARI, ENIGMA, USGS, McMac, GIMA, and U. Tromsø. The focus on SuperMAG is ionosphere-magnetosphere research. It provides easy access to validated measurements of magnetic field perturbations in the same coordinate system, with identical time resolution and a common baseline removal approach. Before SuperMAG, global or even local studies required painstaking and labor-intensive data-handling, which effectively limited research. Analysts faced several inherent complications: confusing or even unknown coordinate systems, a multitude of data artifacts and errors, unknown baselines, and even difficulties obtaining data. These problems have resulted in a serious underutilization of data from magnetometers. With the introduction of SuperMAG, researchers, teachers, students and the public are provided with a practical and time efficient means to study the behavior of the ionospheric and magnetospheric current systems.

[5] Beyond the research community, SuperMAG targets the general public—in particular teachers and students. This puts additional requirements on the site because these groups cannot be assumed to have extensive knowledge of either the data set or the underlying physics. Consequently, the SuperMAG Web Site is based on an intuitive interface with easily accessible, data, plots and derived products.

[6] Ground magnetometers have three observational strengths which make their application particularly useful for monitoring and studying the M-I system: (1) continuous uninterrupted monitoring, (2) nearly global coverage (see Figure 1), and (3) decades of observations.

[7] Studies of the variations caused by electric currents flowing in the ionosphere and magnetosphere require a subtraction of the dominant and slowly varying Earth main field. Hence, both absolute and variometer data (data with unknown baselines) are included in SuperMAG. SuperMAG is truly an excellent example of the saying that "the whole is greater than the sum of all parts."

[8] In section 2, I provide a brief outline of the SuperMAG data flow; in section 3, I show how the local magnetic field coordinate system is determined; section 4 explains my definition of a 'typical' value which has important implications for the entire data processing package; section 5 describes how the baseline is determined and in section 6 the baseline is validated; section 7 is a discussion of the SuperMAG data handling technique and finally section 8 is summary and conclusions.

2. Data and Data Flow

[9] The primary data set is ground based magnetometer data gathered by the SuperMAG collaborators and obtained through the SuperMAG service. The data set is collected by more than 300 magnetometers spread over the entire globe and operated by a long list of organizations and agencies.

[10] In designing the data ingestion system and the data handling software SuperMAG was faced with the challenges of vast amounts of data provided by many different data providers. Each using different data formats, sampling rate,

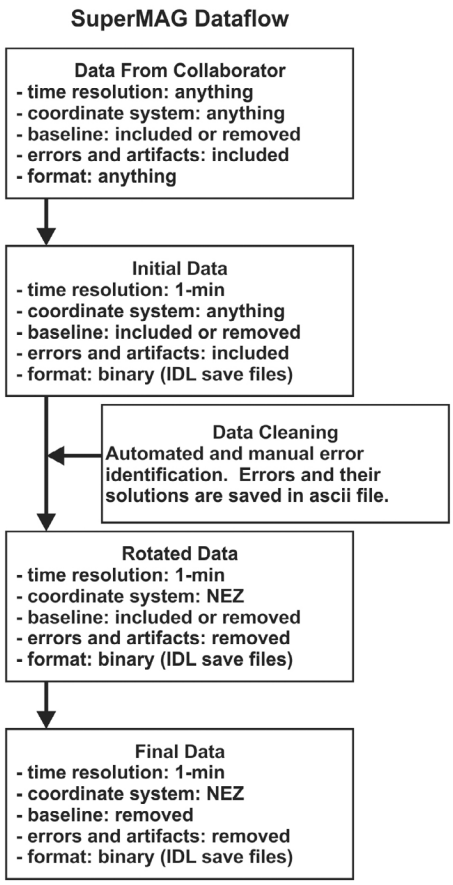

Figure 2. Data flow illustrating the basic steps involved in ingesting data into the SuperMAG system.

data gap indicators, coordinate systems, units and so on. With these complications in mind the SuperMAG data handling system is founded on four basic requirements. The system must (1) be fully automated; (2) be flexible, so new station data from can be included seamlessly; (3) be fully self-contained requiring no additional information (other than the data itself); and (4) not have any hardcoded assumptions in data handling.

[11] The first two requirements are driven by the overwhelming amount of data (>300 stations and decades of data for a total of >15,000 years of 1-min data) and the need for seamless (minimal effort) ingestion of new data from new stations and new data providers. The last two requirements are perhaps less self-explanatory. Ground based magnetometer observations span several decades and for some stations more than a century so the data handling must be fully self-contained since it cannot be expected that any additional information is available. Finally, I required the data handling (i.e., rotation and baseline) not to rely on any, more or less subjective, hard coded assumptions as these may not be applicable to data regardless of origin and date.

[12] Based on the above four requirements a robust data structure and data flow was developed to ingest data in the SuperMAG system (see Figure 2). Data obtained from each collaborator is read by a collaborator dependent program and is resampled to a temporal resolution of 1 min (using centered boxcar average). The resampling is required as data are provided with variable temporal resolution (typically 0.5 s to 60 s). The resampled data are then validated using both an automatic and a manual process. The latter is very labor intensive. The resampled and validated data are rotated into a common reference system (see section 4) and finally the baseline is determined and subtracted (see sections 5 and 6). The flowchart in Figure 2 illustrates the basic data flow starting with data provided by the source and ending with data released to the SuperMAG website. At each step of the process housekeeping plots are produced and a number of validation routines check the quality of the data and the assumptions used in the data processing (see section 6 for validation). Examples of the test made are given in section 4 (coordinate system).

[13] The data cleaning is done both automatically and manually. The latter is very time consuming as ground magnetometer data typically are provided with a long list of errors. Sudden changes in the baseline (offsets), spikes, gradual slopes and other types of errors are abundant in most data sets. While some can be identified and corrected by an automated procedure others require an experienced evaluator. Although SuperMAG uses a massive amount of time on data correction, the user is encouraged to validate the data before using them in presentations and publications. For each station and each year an ascii file is generated which includes a list of identified errors and their solution. This file is used for all subsequent steps in the data processing.

[14] When final data have been processed the files are moved to the server where they are ingested into the SuperMAG website. This is done using an extensive library of routines partially based on the SuperDARN Radar Toolkit. Finally, the Website itself consists of a comprehensive set of software developed for SuperMAG allowing the user to plot and download data and derived products as well as to make custom designed movies. The latter is an example of the first-ever capabilities provided by the SuperMAG website. These last two software packages are not described in this paper but will be discussed in a later paper.

3. Local Magnetic Coordinate System

[15] Global studies require all data to be rotated into a common known coordinate system. Data provided to SuperMAG from the collaborators are typically in either (1) geographic coordinates (typically referred to as XYZ) or (2) geomagnetic coordinates (typically referred to as HDZ).

[16] While the geographic orientation is time independent the Earth main field is constantly changing so the geomagnetic coordinate system is time dependent. This effectively means that for geomagnetic coordinates the orientation of the two horizontal components is unknown. To complicate matters further, all sorts of permutations exist mixing and matching coordinate systems and notations. Likewise, units of the individual component can vary (nT, degrees, radians, minutes) and although the declination supposedly is an angle it is often found to have units of nT. Determining the actual coordinate system is a non-trivial task which in the SuperMAG system is achieved through a series of tests that answer the following questions: (1) Has the baseline been removed? (2) Is the coordinate system geomagnetic or geographic? (3) What are the units of the measurements (nT, degrees,

radians, minutes)? All these issues put serious demands on the users when they attempt to include data from many different providers.

[17] To avoid adding to the already considerable confusion SuperMAG uses a local magnetic coordinate system, the NEZ-system, defined as:

$$\bar{B} = (B_N, B_E, B_Z) \tag{1}$$

where the N-direction is local magnetic north; the E-direction is local magnetic east; and the Z-direction is vertically down. From this coordinate system it is possible to rotate to, for example, geographic coordinates using an IGRF model with the appropriate epoch.

[18] Regardless of the coordinate system of the measurements I rotate the data into this local magnetic coordinate system. The time dependent declination angle is determined by:

$$\theta = \theta(t) = \mathrm{atan}\big(B_{\perp,1}(t)/B_{\perp,2}(t)\big) \tag{2}$$

where $B_{\perp,i}$ is the i'th component of the horizontal field. Assuming that the declination is slowly varying I use a 17 day sliding window to determine a typical value (see section 4 below) and apply a subsequent smoothing.

[19] To illustrate the technique Figure 3 shows the two horizontal components measured from the station HRN before the rotation (Figure 3, top). HRN provides data in the geographic XYZ-system and the declination is only a few degrees as can be seen in Figure 3 (middle). The time dependent declination is shown for 5 consecutive years to illustrate the robustness of the solution and to illustrate the fact that while the declination angle has a slow steady trend it also has a seasonal variation superposed. The trend changes ~0.3 deg/year while the seasonal variation has an amplitude of ~0.2 deg and a period of 12 months. The slow trend is most likely caused by changes in the main field and similar behavior is seen in all stations regardless of latitude/longitude. The seasonal variation is not seen in all stations but the fact that it is repeatable and has a period of 12 months certainly indicate that it is associated with seasonal changes. It may be due to thawing and freezing of the ground on which the magnetometer is founded. Interestingly this seasonal change is not obvious from the raw data but it is very clear in the declination angle particularly when several years are plotted.

[20] The determined declination angle (black) has minor fluctuations around the smoothed solution (red). The deviations are typically <0.05 deg corresponding to an uncertainty of <1 nT for an intense 1000 nT perturbation. This is well within the uncertainty of the measurements (e.g., see Figure 12).

[21] There are a few inherent assumptions in the determination of the declination angle which should be briefly discussed. The first assumption is that the vertical axis is indeed vertical. Luckily, this is technically not difficult to ensure at deployment and errors are a function of sine to the error in the attitude and are therefore small.

[22] The second assumption is that there are no erroneous offsets in either of the horizontal components. Thus, the technique can be used for observatory data which provide absolute measurements of the field but is strictly speaking not valid for variometers as these do not provide absolute measurements. This presents a considerable problem since there is no way to objectively determine the cause of an offset in the Y-component (see Figure 3) as this could be due to an erroneous offset or the actual orientation of the axis. Hence, it is hence worthwhile to estimate the impact of offsets. For measurements using geographic coordinates I have, $B_X \gg B_Y$ for all stations other than near the magnetic pole. If I further make the reasonable assumptions that $B_{X,offset} \ll B_X$ and $B_{Y,offset} \ll B_X$ I can approximate (2) by:

$$\begin{aligned}\theta_{measured} &= \mathrm{atan}\Big[\big(B_Y + B_{Y,offset}\big)/\big(B_X + B_{X,offset}\big)\Big] \\ &\approx \left[\frac{B_Y}{B_X} - \frac{1}{3}\left(\frac{B_Y}{B_X}\right)^3\right] + \left[\frac{B_{Y,offset}}{B_X} - \left(\frac{B_Y}{B_X}\right)^2\left(\frac{B_{Y,offset}}{B_X}\right)\right] = \theta + \theta_{error}\end{aligned} \tag{3}$$

ignoring all terms small by second order or more. According to (3) I only need to be concerned with the Y-component offset and can ignore the X-component offset as the contribution is small of second order. The first square bracket is the real declination while the second is the error introduced by the offset. As the real declination, θ, can be zero it is irrelevant which is larger. It is, however, important to estimate the error, θ_{error}, introduced by the offset. As equation (3) shows the error is proportional to $B_{Y,offset}$ / B_X. The error in the declination introduces an error in the two horizontal components since the coordinate system is misaligned. However, the error will lead to a negligible error in the direction of the ground perturbation (typically the N-direction) and we can now estimate the error in the direction perpendicular to the ground perturbation (typically the E-direction).

[23] The error in (3) is proportional to the magnitude of the perturbation. Both the size of the perturbation and B_X have a clear latitudinal dependence (B_X decreases toward the magnetic pole while the magnitude of the ground perturbations maximizes in the auroral zone) and I can estimate the error using some typical values. Assuming $B_{Y,offset}$ = 100 nT: (1) polar cap: For B_X = 4000 nT I get $\theta_{error} \approx$ 1.5 deg corresponding to an error of ~2 nT for an intense 100 nT event; (2) auroral zone: For B_X = 12,500 nT I get $\theta_{error} \approx$ 0.45 deg corresponding to an error of ~8 nT for an intense 1000 nT event; and finally, (3) sub auroral zone: perturbations are small and the horizontal field is strong and thus I can ignore θ_{error}. As I show later in the paper these worst case uncertainties are far smaller than the variability of the system (e.g., see Figure 12) and can thus be ignored for studies of the magnetosphere-ionosphere system. Operators of ground magnetometers should, however, attempt to keep offsets small (or at least know their magnitude) as they do introduce an uncorrectable error.

4. Determining a 'Typical' Value for a Distribution

[24] Throughout the paper I am faced with the problem of determining a single scalar value which is representative of a series of numbers. As I will show using an average value is not sufficient for the problems the paper is dealing with. I will refer to this value as a 'typical' value. Needless to say a single scalar cannot represent a vector with a certain probability distribution but for the purpose of the data handling it is required that a value is determined. Further complicating the

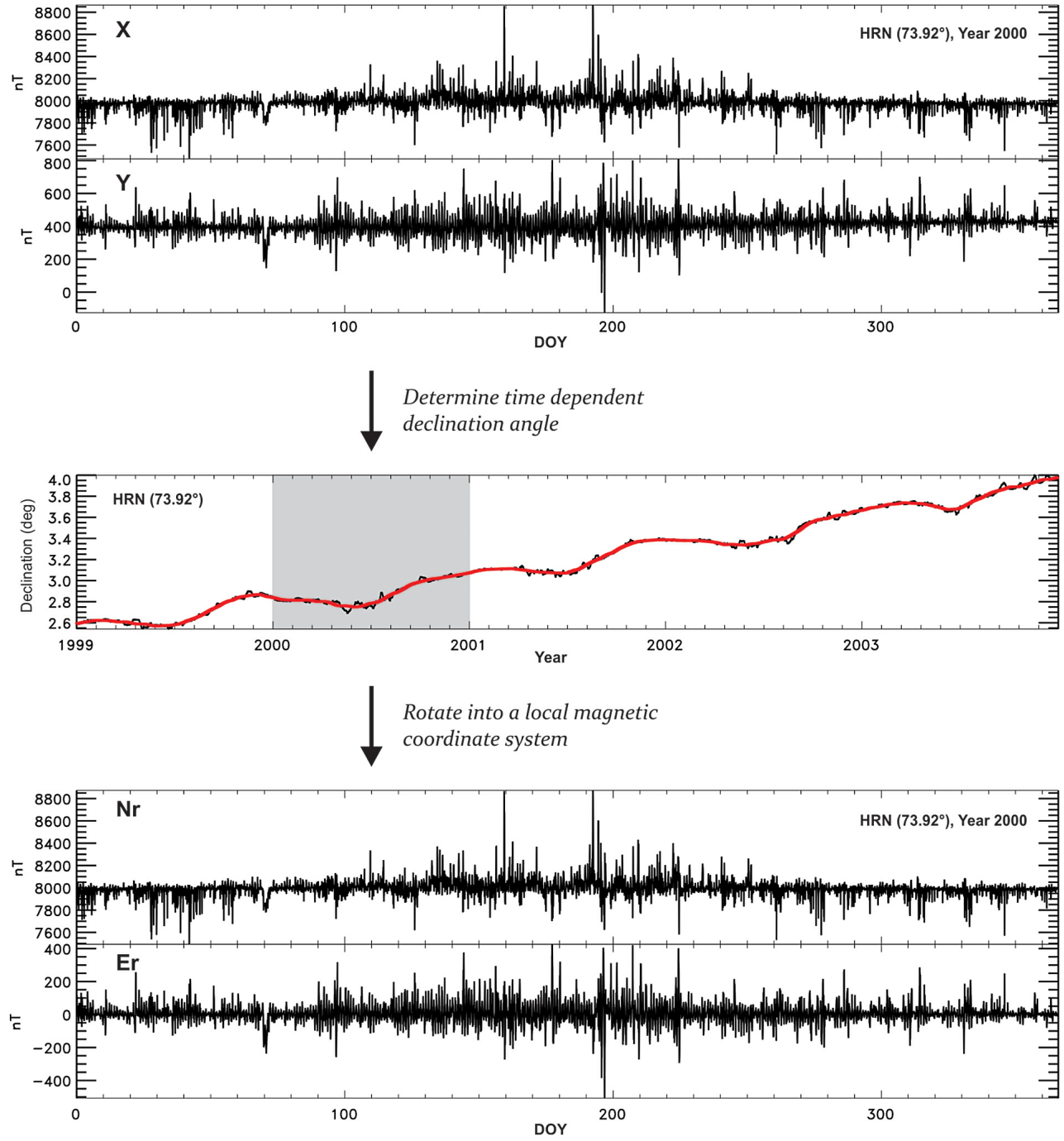

Figure 3. Measured horizontal components for the year 2000 (top) before and (bottom) after a rotation into a local magnetic coordinate system. (middle) The declination angle for a five year period (gray area indicates the year 2000).

problem of determining such a number is the fact that a time series of ground magnetometer data rarely produces a symmetric probability distribution. This is particularly the case for the N-component at any latitude since the ring current and the dominant auroral electrojet component (the westward electrojet) both produce negative N values and thus skew the distribution. It is, therefore, pertinent for the remainder of the paper that I clarify how I determine the 'typical' value.

[25] Figure 4 shows a typical 16 day time series for the N-component (station is ABG located at low magnetic latitudes) and the probability distribution. An intense magnetic storm occurred in the middle of this interval producing very strong perturbations. As mentioned above the probability distribution is clearly not symmetric (skewness is not zero) and large negative values are present. Four different values are indicated on the plot: (1) the average (red), (2) the median (blue), (3) the center of a Gaussian fit (green), and (4) the

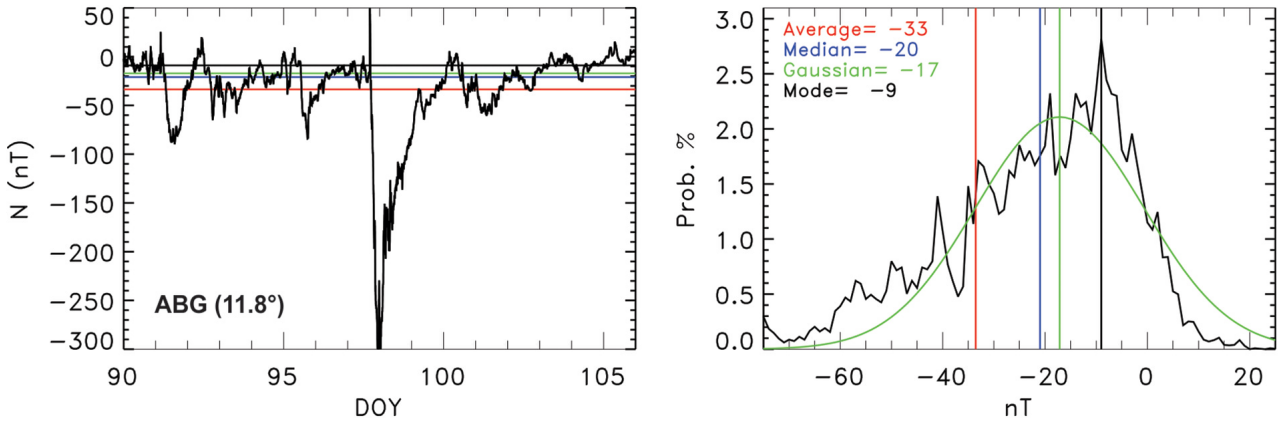

Figure 4. (left) A 16 day interval of the N-component for an equatorial station and (right) the probability distribution. The average (red), the median (blue), the center of a Gaussian fit (green) and the mode (black) are indicated on both plots.

mode (black). The nonzero skewness and large negative values affect the average and the mean while the Gaussian and the mode is less sensitive to these non-common values. Based on this typical example I conclude that for ground magnetometer data neither the average nor the median provides values that can be referred to as 'typical'.

[26] To find our 'typical' value the probability distribution is derived, the mode is determined and a Gaussian is fitted (least squares). The typical value is defined as the mode unless the following requirement is fulfilled:

$$\mu > \sum_{i=-1,1} f_i/3 \tag{4}$$

where μ is the magnitude of the Gaussian, and $f_0 \equiv M_0$, is the most commonly occurring value or mode. This simple nearest neighbor averaging of the binned data is introduced to take care of single point spikes. This is used to handle constant (erroneous) data which produce a single spike in the probability distribution. The mode and the magnitude of the Gaussian fit typically produce very similar values.One minor caveat should be mentioned though. The mode is not necessarily a single number (although in this application it almost always is) so I define the mode, M_0, as a simple average of the individual modes M_i:

$$M_0 = \frac{1}{n}\sum_{i=1,n} M_i \tag{5}$$

When I refer to the 'typical' value it has been determined using the above procedure.

5. Baseline Determination Technique

[27] In this section I outline the technique for determining the so-called baseline. My technique is a break from traditional methods which are based on the identification of quiet days and followed by some sort of smoothing and extrapolation to disturbed days. Section 7 provides a discussion of these techniques.

[28] The purpose of determining the baseline is to make a separation of sources. The measured field on the surface of the Earth is due to a list of sources:

$$\bar{B}_{measured} = \bar{B}_{main} + \bar{B}_{Sq} + \bar{B}_{FAC} + \bar{B}_{RC} + \bar{B}_{EJ} + \bar{B}_{MP} \ldots \tag{6}$$

where the right side terms indicate the contribution due to: The Earth main field; the *Sq* current system; the field-aligned currents; the ring current; the auroral electrojets; and the magnetopause currents.

[29] The focus of SuperMAG is ionosphere-magnetosphere research so perturbations produced by currents flowing in and between the ionosphere and the magnetosphere should be maintained while all other sources to the measured field should be removed. According to Ampere's law it is impossible to determine a single unique current solution from the measured field. It is, however, possible to make a separation of sources if reasonable assumptions are made. For example, that the Earth main field is slowly varying compared to all other sources.

[30] In my definition the baseline consists of two components: (1) a slowly varying offset or trend which is mainly but not solely due to the Earth main field and (2) a diurnal component which is mainly, but not solely, due to the *Sq* current system.

[31] While the *Sq* current system is produced by an ionospheric current I choose to remove it nevertheless. My technique aims at removing both these contributions without removing the contribution produced by the external currents. As my baseline determination is based on the observations themselves without any additional information it follows from 1 and 2 that the determination is complicated by external field contributions that either varies slowly (comparable to the main field variability) or has a significant diurnal component. This is discussed, for example, in section 6.2.

[32] The baseline for any given station and component is determined in three steps using a full year of observations: (1) determine the daily variations, (2) determine the yearly trend,

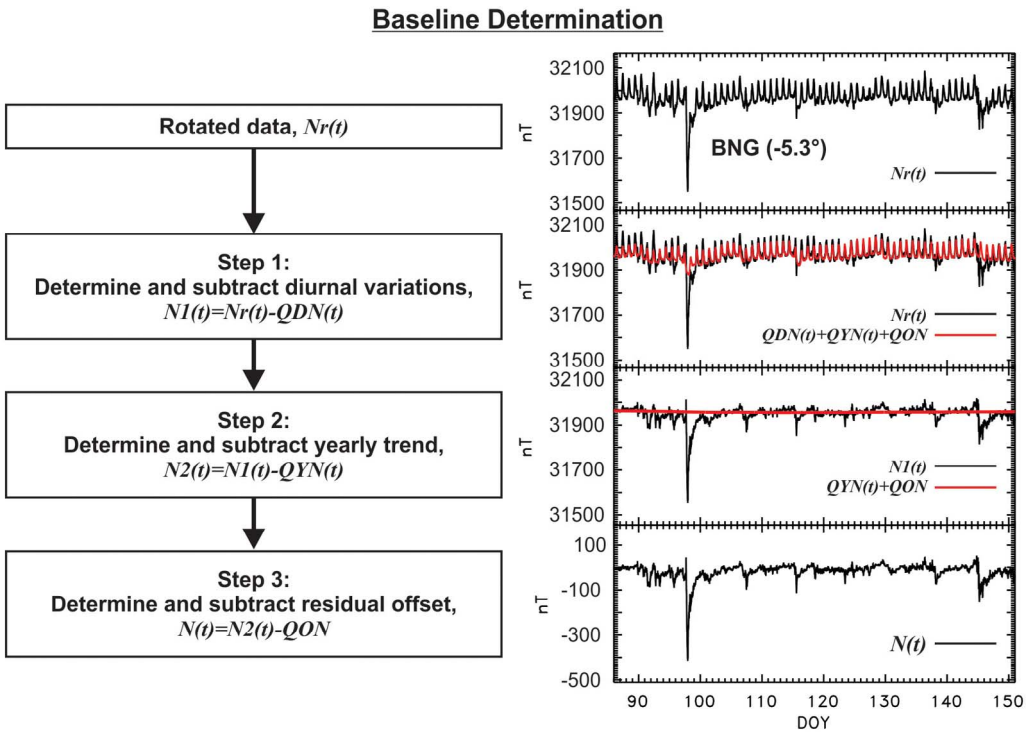

Figure 5. Data flow illustrating the basic steps involved in determining the baseline and a 65 day interval illustrating the steps. Data from BNG year 2000 are used for illustration.

and (3) determine any remaining offset. Thus, I remove the baseline from the N-component as:

$$N(t) = Nr(t) - QDN(t) - QYN(t) - QON \qquad (7)$$

where $Nr(t)$ is the rotated N-component, $QDN(t)$ is the daily baseline, $QYN(t)$ is the yearly trend, and QON is the residual offset. Below I explain how each of the three baseline contributions is determined. Throughout the description and in the figures I refer to the N-component to illustrate the technique. The E- and Z-components are treated exactly the same. It should also be mentioned in passing that although I use a full year of data the technique is not affected by data gaps and the ends of the vector, $N(t)$, are treated by including data from neighboring years.

[33] Figure 5 (left) shows a flowchart outlining the procedure, and Figure 5 (right) shows the associated plots from a 65 day interval. The data were obtained during a time interval when an intense magnetic storm occurred. Measurements were made at equatorial latitudes and a strong diurnal component is present in the rotated data (first panel in Figure 5 (right)). The daily variations and the trend are superposed in the second panel (red line). In the third panel the daily variations have been subtracted (black line) and the yearly trend is superposed (red). Finally, in the fourth panel all three baseline contributions have been removed. Comparing the first and fourth panels it should be clear that while diurnal variations and the trend have been removed, both short duration variations (such as substorm signatures) and long duration events (magnetic storms) are maintained. The performance of the technique can be illustrated further by plotting the power spectra before and after the baseline has been removed (Figure 6). Notice the diurnal, the second, third and fourth harmonics in Figure 6 (top). These peaks are all absent in Figure 6 (bottom) so the baseline removal technique effectively eliminates diurnal variations supporting the conclusion from Figure 5. It should be mentioned, that not all harmonics are present at all stations/components and that for auroral latitudes the first harmonic is present even after the baseline subtraction. This is, however, expected as the westward and eastward electrojets are more or less fixed in local time and thus produce a diurnal variation that should not be removed (for an extensive discussion and validation see *Newell and Gjerloev* [2011a, 2011b]). The two findings

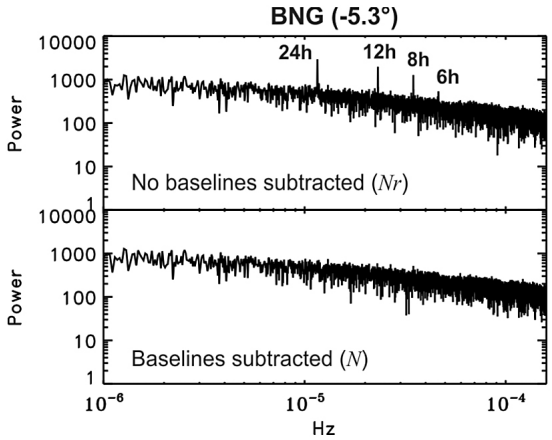

Figure 6. Power spectra (top) before and (bottom) after the baseline has been removed (BNG year 2000). Notice the diurnal and second, third and fourth harmonics (top). These are all removed by the baseline.

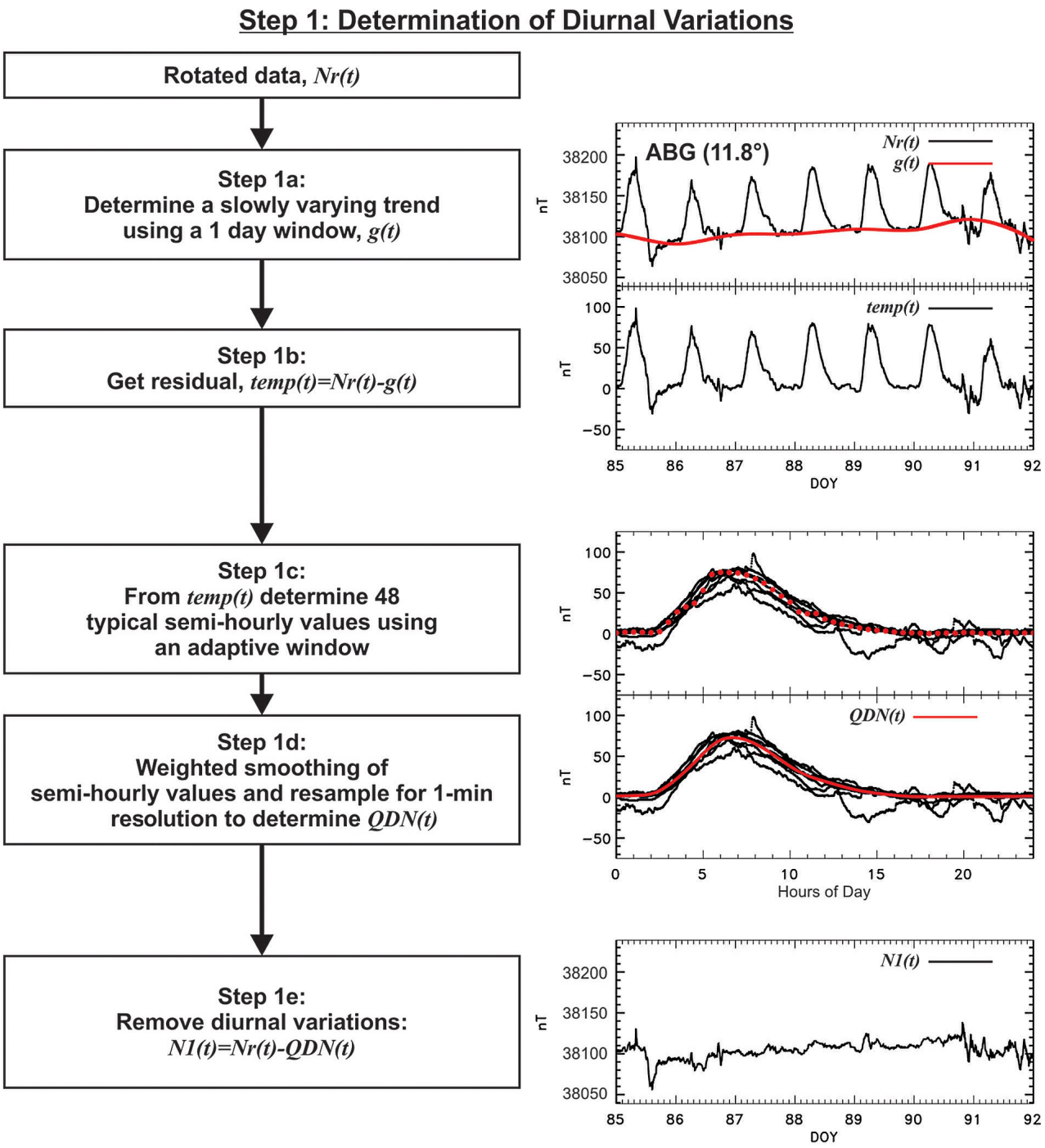

Figure 7. Data flow illustrating the basic steps involved in determining the daily baseline and a 7 day interval illustrating the steps.

strongly indicate that a simple bandstop filtering of the data (centered at 24 h periods) cannot be used as it will not eliminate the diurnal variations (higher harmonics) and/or remove the external field which I am trying to maintain (auroral latitudes).

5.1. Step 1: Determination of the Diurnal Variations, QDN(t)

[34] Figure 7 shows the five basic steps by which the diurnal variation is determined and in this section I explain how each step is performed. There are a number of possible sources that produce diurnal variations. This includes the well-known *Sq* current system but also artifacts that may have a local time dependence (i.e., temperature dependence). This step aims at removing all contributions to the observed diurnal variations – real or instrumental.

5.1.1. Steps 1a and 1b

[35] In order to isolate the diurnal variations from the measured field I must first remove the field that varies on time scales longer than 1 day (Step 1a). Figure 7 (top right)

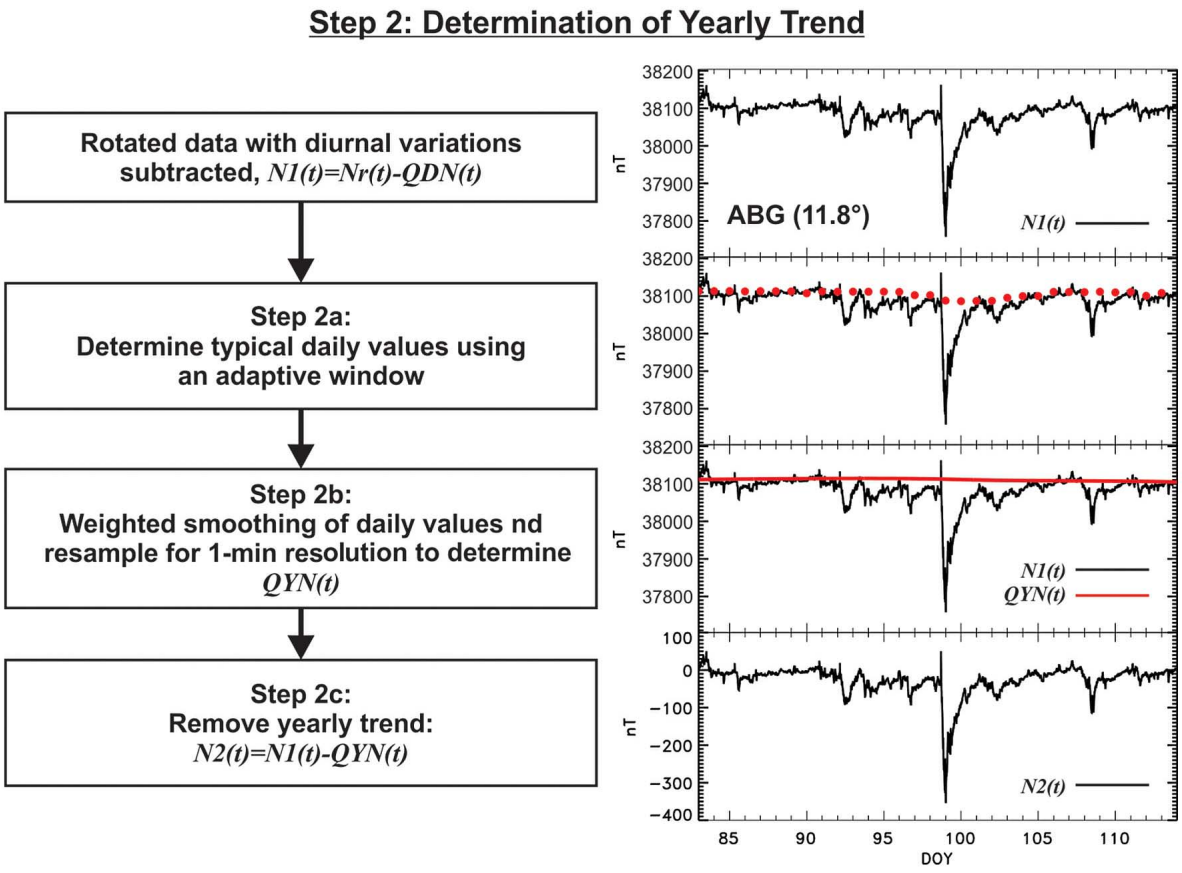

Figure 8. Data flow illustrating the basic steps involved in determining the yearly baseline and a 36 day interval illustrating the steps. Data from BNG year 2000 are used for illustration. Data from ABG year 2000 are used for illustration.

shows measurements from an equatorial station clearly illustrating the problem with a diurnal variation (amplitude of ~80 nT) superposed on a slowly varying trend (red line). The trend, $g(t)$, is derived by determining the typical value for each day. $g(t)$ is then resampled from the 24 h resolution to a 1-min resolution using a cubic convolution interpolation method [*Park and Schowengerdt*, 1983]. In step 1b the trend, $g(t)$, is subtracted from the rotated data (second panel in Figure 7 (right)).

5.1.2. Step 1c

[36] From the residual, $temp(t) = Nr(t) - g(t)$, I determine the diurnal variations. This is done by including data from 3 days (day in question plus neighboring days) and determining a typical value for 30 min intervals (third panel in Figure 7 (right)) resulting in 48 discrete values per day. If there is too much scatter in a given 30 min interval (90 points) the 3 day window is symmetrically widened by two days. This is repeated until a solution is found. The solution is accepted if a Gaussian fit to the probability distribution obeys:

$$\sigma < FWHM_{statistical} \tag{8}$$

where σ is the standard deviation of the Gaussian fit and the right hand side refers to the statistical solution shown in Figure 10 and discussed in section 6. Thus, acknowledging the poor statistics (90 points from a 3 day window) I accept a standard deviation of the Gaussian fit that is ~2.3 times the statistical standard deviation (see section 6).

5.1.3. Step 1d

[37] From the semi-hourly values determined in Step 1c (section 5.1.2) I determine the final solution using a weighted fit. The weights are determined from the knowledge of each semi-hourly fit. As discussed above each semi-hourly value also provides knowledge of the spread in the data and the width of the window used. For example, if a particular value required an 11 day wide window before a solution was found the uncertainty is defined as greater than a value determined using a 3 day window.

[38] A final resampling from semi-hourly time resolution to 1-min resolution is done using the cubic convolution interpolation method [*Park and Schowengerdt*, 1983].

5.2. Step 2: Determination of the Yearly Trend, QYN(t)

[39] Figure 8 show the three basic steps by which the yearly trend is determined and in this section I explain how each step is performed. The main contribution is the time dependent Earth main field. In section 4 I found that the declination angle displayed a slow change due to the change of the Earth main field but pointed out that it also displayed a

pronounced seasonal dependence. The latter is clearly not due to changes in the Earth main field but rather due to changes in the daily average temperature and can thus be viewed as an artifact that also needs to be removed. This seasonal variation should not be confused with the real seasonal dependence of the M-I current system which is maintained by the baseline determination technique.

5.2.1. Step 2a

[40] Daily typical values are determined using a 17 day sliding window. For each day a typical value is determined using all data from within the window. As for the daily baseline the window size is increased by 2 days if the solution does not obey (7). The 17 day window may appear to be an arbitrary choice. This is in fact not the case. The window size is a compromise between retaining seasonal changes and ensuring that the baseline is insensitive to the buildup and decay of the ring current. Based on a series of validation runs producing plots (as seen in Figure 11) the 17 day window was chosen as a sensible compromise. In Figure 8, the second panel shows the values for each day (red dots). The solution appears to be affected by the intense magnetic storm showing a minor decrease around DOY = 100. This is not caused by the large negative values. The preceding 7 day depression and the following extended recovery phase is the reason for the minor decrease in the solution. This is an artifact and will be taken care of in the following step.

5.2.2. Steps 2b and 2c

[41] From the daily values determined in Step 2a (section 5.2.1) I determine the final solution using a weighted fitting procedure. The above mentioned ~10 nT (second panel in Figure 8) artifact is removed in the final fit (third panel, red line) using a weighted smoothing procedure. This non-trivial weighting is discussed in section 7.1 but can be briefly explained here. The uncertainty for a given data point is defined by two parts: (1) the instantaneous variance and (2) a scaled variance determined from the history of the data. As illustrated by Figure 8, this procedure corrects the problem and ensures that the baseline does not fit to the long duration magnetic storm. It should be emphasized that this is only a problem for the N-component. For the E-component the problem is negligible (no storm time long duration perturbations) and for the Z-direction the problem is minor (the ring current produces smaller perturbations compared with the N-component).

[42] As for the daily baseline the final resampling from daily values to 1-min resolution is done using the cubic convolution interpolation method [*Park and Schowengerdt*, 1983].

5.3. Step 3: Determination of Residual Offset, QON

[43] A final step removes a possible residual offset, *QON*. This offset is determined from the probability distribution using official quiet days (see section 6.1 for a discussion of this concept). The assumption is that the typical value during quiet conditions is zero. Any offset (*QON*) is subtracted from the entire data set. Figure 9 shows *QON* for all stations for each component as a function of magnetic latitude. On average the offset is small and perhaps insignificant given the typical magnitude of the perturbations. More interesting is the clear latitudinal dependence of the N-component (~5 nT at equator) which may be interpreted as a weak residual ring current being present [see also *Newell and Gjerloev*, 2012] even during these officially quiet days. Assuming the ring current is the cause the *QOZ* should show a similar dependence on latitude (although increasing toward the pole). The Z-perturbation, however, changes sign from southern to northern hemisphere which has been included in the plot. The amplitude of *QOZ* is about half of *QON*. Careful Biot and Savart numerical integrations show that a symmetric ring current at a distance of 5 R_E produces a difference in amplitude between equator and the pole of only ~10%. Far smaller than the observed ~50%. However, moving the ring current closer to the Earth and/or assuming it to be asymmetric produces ground perturbations in agreement with the observed. Interestingly, *Soraas and Davis* [1968] modeled the ring current and found a 5 nT offset in the ground magnetometer observations at equator and interpreted this as being due to a weak quiet times ring current (also F. Soraas, private communication, 2012).

6. Validation of Baseline Technique

[44] To perform a validation analysis I must compare with a different technique. The most widely accepted technique is the use of the official quiet days. In this technique the baseline is defined by the measurements from a quiet day, these are then smoothed and subtracted from surrounding disturbed days. Since this technique is widely used it is reasonable to evaluate the performance of my baselines by comparing them to the measurements on the official quiet days. The list I use is released by Geo Forschungs Zentrum (GFZ) Potsdam (http://www-app3.gfz-potsdam.de/kp_index/qddescription.html; also Kyoto WDC). A brief explanation of how these days are determined can be found on the above site and is discussed in section 7.1.

[45] For a direct comparison between my baseline and the measured field on an official quiet day I use a fortuitous interval where three subsequent days (Feb 17–19, 2000) were labeled as quiet. Figure 10 shows the measured N components (black) and my automatic baseline (red) for three stations (polar cap, auroral and sub-auroral latitudes). For each station I also show the difference between these baselines:

$$diff(t) = \left[Nr(t)\right] - \left[QDN(t) + QYN(t) + QON\right] \qquad (9)$$

where all terms on the right side are defined above. If I limit my calculation of *diff* to official quiet days the first square bracket term on the right side is the classical 'quiet day baseline' while the second square bracket is my baseline. Thus, if the two techniques produce identical baselines I get *diff*(*t*) = 0. Note that the range on the *y* axis is identical for observations and difference but it differs from station to station. Two important points should be apparent from this example: (1) My baseline follows the trend of the observations and (2) there are fairly intense events even on so-called quiet days. The latter finding puts questions at the classical quiet day baseline. The events centered at DOY = 48.6 and DOY = 50.4 peaked at SML = −670 nT and SML = −492 nT respectively (SML is equivalent to AL [see *Newell and Gjerloev*, 2011a, 2011b]).

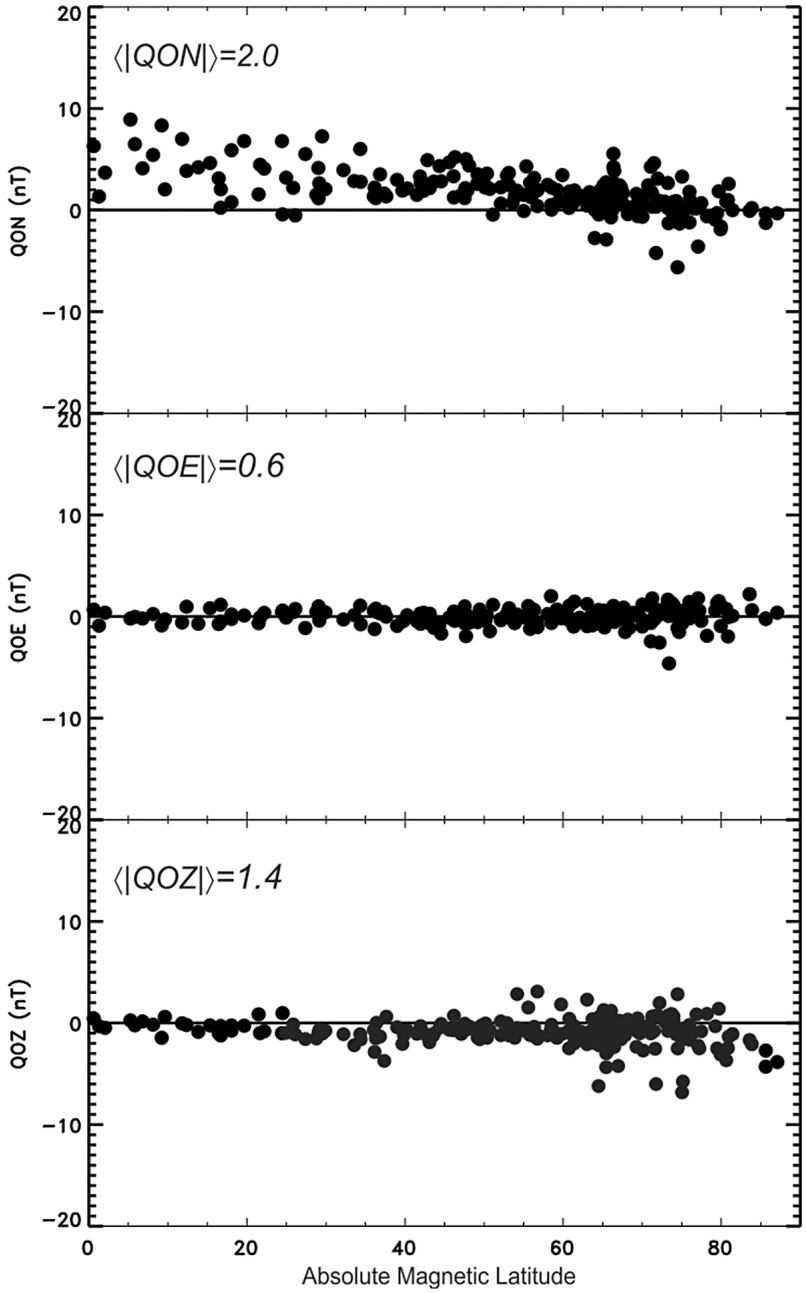

Figure 9. Quiet day offset of the baseline subtracted data. The mean of the (absolute) offsets are indicated. All available stations (year 2000) are included.

[46] To perform a statistical evaluation of the baseline technique I determine the probability distribution of *diff* using the 60 official quietest days for the year 2000 and for all stations. I include all 1440 data points from each of the quiet days and apply no smoothing or filtering. Thus, disturbance events as those evident in Figure 10 are included. Figure 11 shows the probability distribution of *diff* for a midlatitude station and the calculated *FWHM* is also indicated. Making the simplistic assumption that these distributions can be approximated by a Gaussian I find the standard deviation to be 7.5/4.0/3.5 nT for each component. Figure 12 shows the scatterplot of the *FWHM* of the differences, *diff*, for all stations. Figure 12 (left) includes all data while Figure 12 (right) shows the same but for quiet days only. As expected the quiet days result in a smaller *FWHM*, but perhaps more interestingly is the repeatable pattern across all latitudes. This allows me to make a simple fit (indicated in Figure 12 (left)). For the quiet days the standard deviation is roughly 7/4/3 nT (sub-auroral) and 10/7/8 nT (auroral zone) for the N/E/Z components respectively. Considering the above mentioned limitations to the two techniques I conclude this to be nothing short of remarkably good agreement and argue that this serves as a validation of my technique (see discussion regarding the fundamental problems of validating any baseline

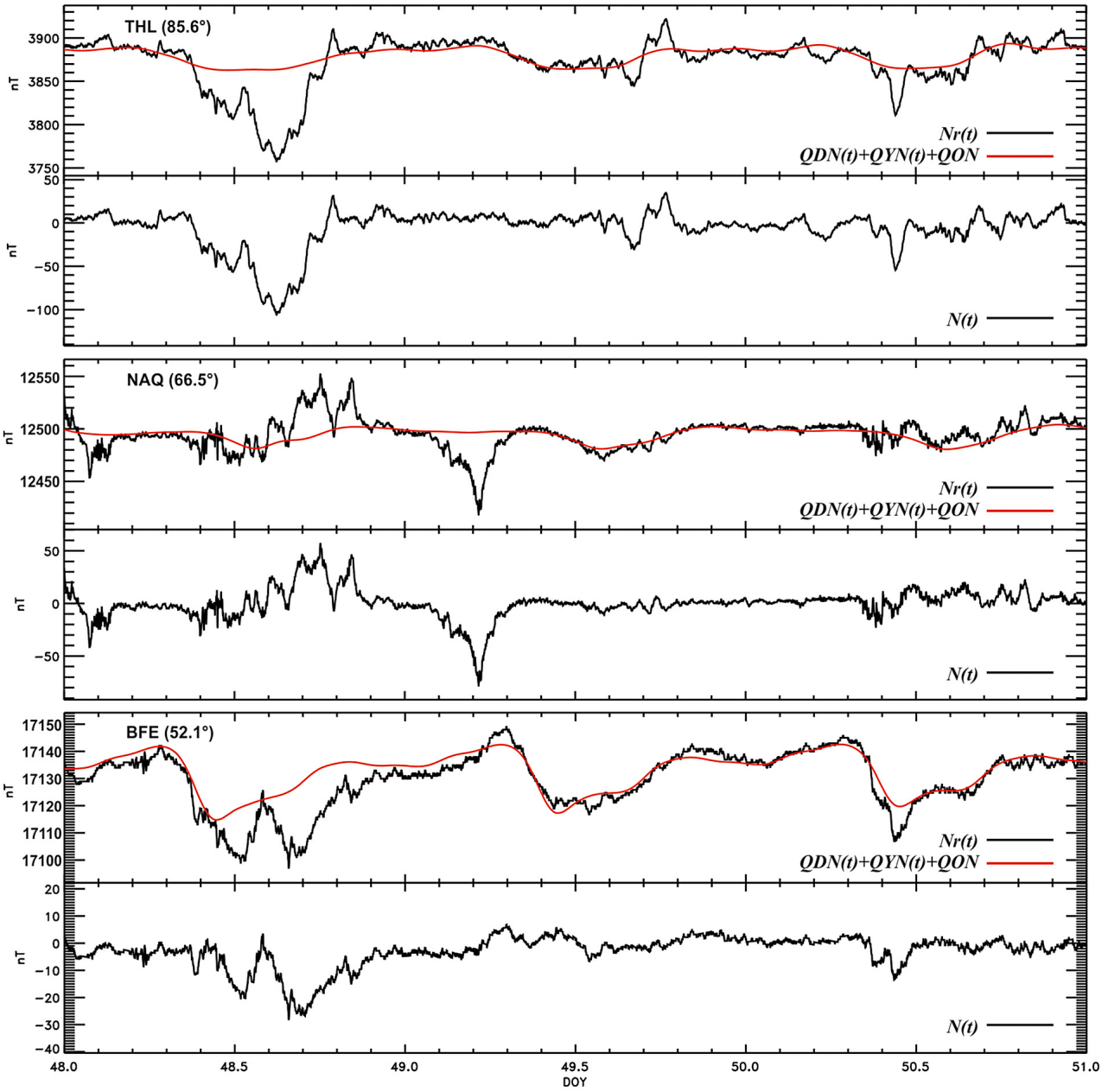

Figure 10. N-component for three stations located within the polar cap, auroral zone and sub-auroral zone with final baselines superposed (red). The three day interval is an official quiet day interval (Feb 17–19, 2000). For each station the top plot shows the rotated N component with the baseline superposed (red) and the residual.

technique). Also, shown are fits based on a linear and a Gaussian component:

$$FWHM(mlat) < \begin{cases} 30 - 0.20 \cdot mlat + 17 \cdot \exp(-(mlat - 76)^2/100), & N\,component \\ 7 + 0.12 \cdot mlat + 14 \cdot \exp(-(mlat - 78)^2/150), & E\,component \\ 5 + 0.13 \cdot mlat + 19 \cdot \exp(-(mlat - 78)^2/150), & Z\,component \end{cases} \quad (10)$$

where *mlat* is the magnetic latitude of the station. Note that the N-component error decreases as a function of latitude until auroral latitudes. This is expected as the ring current contribution decreases as cos(*mlat*) while the reverse is true for the Z-component which increases as sin(*mlat*). This argument indicates that for quiet days the slope is vanishing as is indeed the case (Figure 12, right). The positive slope of the Y-component is somewhat more complicated but is likely

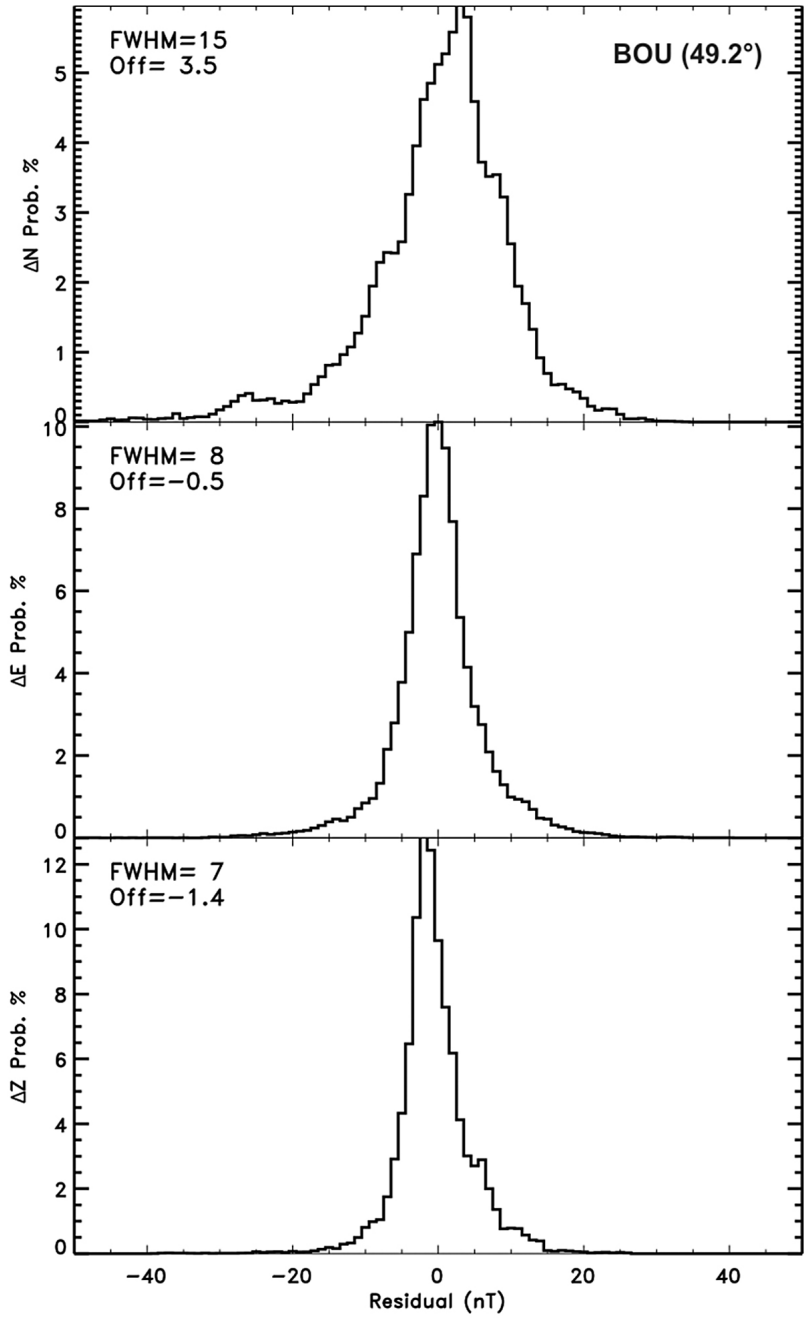

Figure 11. The probability distribution of differences between my baseline and official quiet days (see Figure 10 also).

due to latitudinal dependence of the ground perturbation caused by field-aligned currents connecting the auroral zone and the high altitude magnetosphere.

6.1. Is the Baseline Technique Applicable to All Latitudes?

[47] The statistical properties (e.g., magnitude and temporal variability) of the ground level magnetic field perturbations have a pronounced latitudinal dependence. Based on these differences I can separate the ground magnetometers into three basic groups: sub-auroral stations, auroral zone stations, and polar cap stations. It is thus pertinent to address the performance of the baseline technique for each of these groups. A visual inspection of Figure 10 may be used to argue that the baseline technique provides a reasonable solution regardless of latitude – at least for these stations and this time interval. Additionally, Figure 12 showed that the spread in the data, *FWHM*, was well behaved as a function of latitude and thus across the three latitudinal ranges. This also provides an argument for the validity of the technique regardless of the latitude of the station. Finally, I wish to emphasize that there are no hardcoded inherent assumptions in the technique and

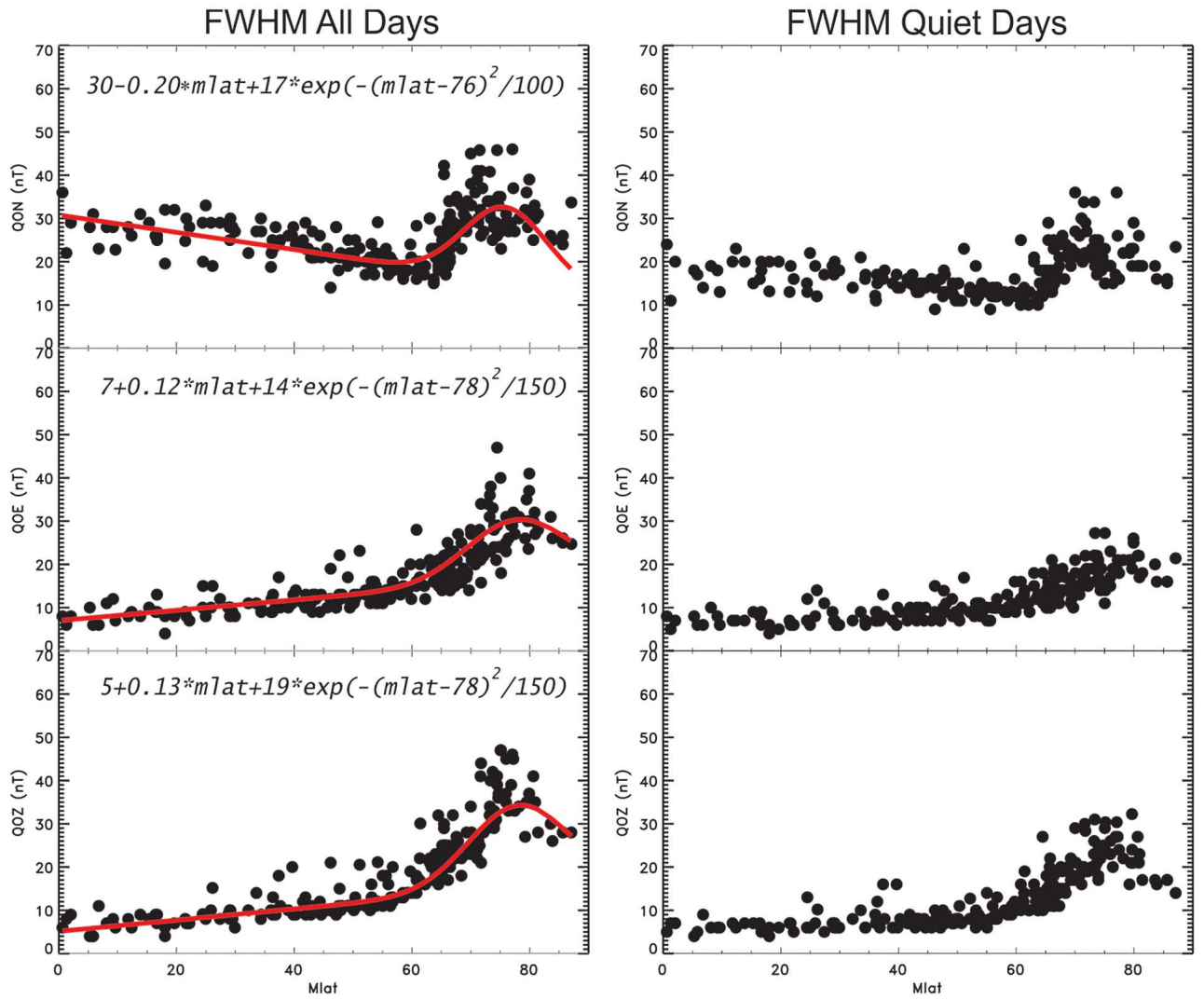

Figure 12. The *FWHM* of the distribution (left) for all data and (right) for data obtained during official quiet days. Each dot indicates the *FWHM* for a station (year 2000). Note that the uncertainty has a pronounced dependence on magnetic latitude and component.

thus all stations and all components are treated similarly regardless of latitude.

6.2. Long Duration Magnetic Storms

[48] The energization and subsequent decay of the ring current present a particular difficult problem for a baseline determination due to the long time scale. The typical time scale for magnetic storms is days but they can last more than a week. For the baseline determination the problem is the symmetry of the ring current which produces a more or less constant negative perturbation in the low latitude N-component which is dominant at those latitudes. The Z-component at high latitudes is easier to handle as the contribution from the highly variable auroral electrojets is far greater than the ring current perturbation. *Newell and Gjerloev* [2012] addressed this by deriving partial ring current indices based on SuperMAG data so I refer to their paper for an extensive validation and analysis of this problem.

[49] Figure 13 shows the N-component from a low latitude station (ABG) during the intense April 6 2000 storm and the SYM-H index. Considering that SYM-H is derived from 6 stations with a latitude correction and that ABG is a single station making single point measurements with a UT dependence, I find the SYM-H and N-component to be in remarkable agreement. It should also be clear that there is no sign of the baseline (incorrectly) fitting to the long duration storm despite the fact that the SYM-H is depressed for a staggering 29 days (DOY = 84 to DOY = 113).

7. Discussion

[50] It is often asked: What is the correct baseline and how can it be determined? In the SuperMAG data processing technique the baseline determination is unquestionably the most difficult and controversial problem. In the literature the baseline is often referred to as the 'quiet day curve', *QDC*, or the 'solar regular variation', S_R. A number of papers have tried to determine the *QDC* or S_R using various techniques [e.g., *Mayaud*, 1980; *Menvielle et al.*, 1995; *Takahashi et al.*, 2001; *Janzhura and Troshichev*, 2008]. Common for these is

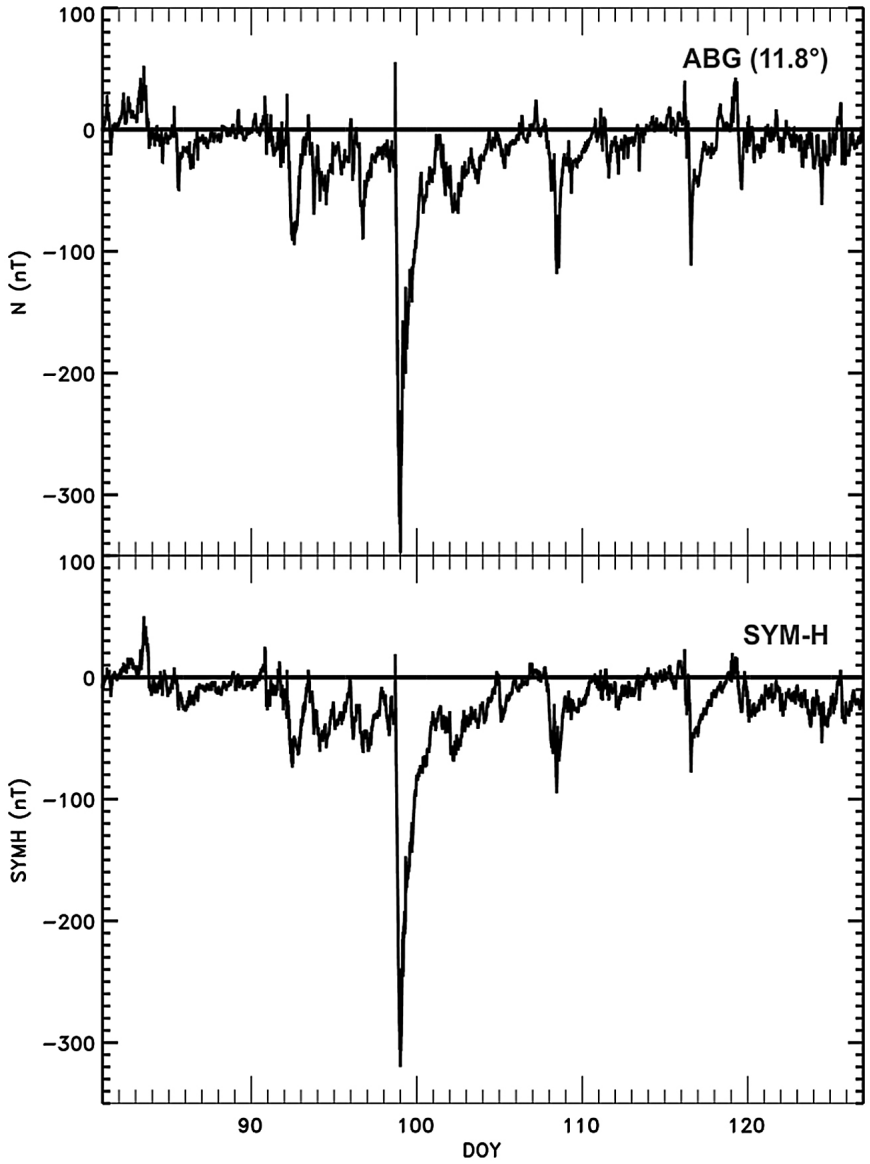

Figure 13. (top) N-component after baseline subtraction for a 46 day interval (year 2000) during which an intense magnetic storm occurred. (bottom) SYM-H for the same interval.

the identification of so-called quiet days defined as 24 h periods starting at 0 UT. These periods define the *QDC* which are then used for adjacent disturbed days (applying some sort of smoothing and extrapolation technique).

[51] It is beyond the scope of this paper to provide a full review of the many published techniques used to determine which days are quiet and which are disturbed (e.g., the excellent review monograph by *Mayaud* [1980]). However, for here it is important to repeat the technique used by Geo Forschungs Zentrum (GFZ) Potsdam as it is the most widely used: "The selection of the quietest days (Q-days) and most disturbed days (D-days) of each month is deduced from the Kp indices on the basis of three criteria for each day:

[52] 1. The sum of the eight Kp values.

[53] 2. The sum of squares of the eight Kp values.

[54] 3. The maximum of the eight Kp values.

[55] According to each of these criteria, a relative order number is assigned to each day of the month, the three order numbers are averaged and the days with the lowest and the highest mean order numbers are selected as the five (respectively ten) quietest and the five most disturbed days.

[56] It should be noted that these selection criteria give only a relative indication of the character of the selected days with respect to the other days of the same month. As the general disturbance level may be quite different for different years and also for different months of the same year, the selected quietest days of a month may sometimes be rather disturbed or vice versa."

[57] Thus, the technique acknowledges that the selected quietest days can include intense substorms (as illustrated by Figure 10 which included substorms for which SME and AE exceeded 500 nT). Anecdotally, the use of 5 days per month rather than any other number is a decision made more than a century ago by the International Commission in 1905 at a time when our understanding of the M-I system was sketchy at best.

[58] *Joselyn* [1989] discussed several published methods for selecting quiet days and identified three caveats (rewritten and shortened):

[59] 1. The finite station coverage may miss a disturbance event.

[60] 2. Geomagnetic indices are convenient but imperfect indicators of geomagnetic activity.

[61] 3. Geomagnetic activity does not fully reflect the range of possible factors that influence the ionosphere or magnetosphere.

[62] While these certainly are valid concerns I add three additional issues:

[63] 4. Using any geomagnetic index (e.g., Kp) to identify quiet days involves a circular argumentation as the derivation of these indices require that a baseline has been subtracted from the measurements.

[64] 5. There is no logical argument that a 24 h quiet period should begin at 0 UT. While this may be practical it is certainly not derived from any arguments based on solar wind-M-I system physics.

[65] 6. The use of a 24 h window is in conflict with the reconfiguration time of the M-I system and a quiet day can therefore include significant disturbances.

[66] For additional discussion of a number of other caveats and concerns see *Mayaud* [1980] and *Menvielle et al.* [1995].

[67] The reconfiguration time of the M-I system is known to be roughly 10 min [e.g., *Gjerloev et al.*, 2011] which is the time it takes for the magnetosphere to undergo a large-scale reconfiguration for example from a stretched configuration to a more dipolar configuration. It, thus, seems irrational to use a wide window with the size of 24 h. While the 24 h window is in agreement with the *Sq* current system it is not in agreement with the variability of the M-I system. As a consequence quiet days should not be mistaken for days with vanishing M-I currents as illustrated by Figure 10 (which included significant substorms despite being official quiet days). Thus, they are not well suited for studies of the M-I current system as they cannot provide the desired separation of sources.

[68] The question as to how the baseline should be determined is still under debate as evident from the stream of new papers being published which attempt to derive the *QDC* [e.g., *Mayaud*, 1980; *Menvielle et al.*, 1995; *Takahashi et al.*, 2001; *Janzhura and Troshichev*, 2008]. The fundamental problem is that there is no objective way to evaluate the quality of each technique. In validating any result or technique it is required that a set of ground-truth observations exists. Agreeing with another set of results does not provide an argument of validity as both could be erroneous. This is particularly true for baseline determination as just about any data provider and as many scientists have developed their own technique.

[69] As mentioned in section 5 the purpose of the baseline determination is fundamentally to perform a separation of sources. As there is no objective way to separate the sources neither is there a way to perform an objective evaluation. Returning to the above question (beginning of section 7) I therefore conclude that the question is poorly stated and irrelevant. The user of the data must keep in mind the assumptions used in the baseline determination and draw conclusions accordingly.

7.1. Determining Variability

[70] I overcome the above mentioned problems (and many additional) inherent to the quiet day approach by simply avoiding the use of them. I do, however, need an estimate of the uncertainty of the data. To determine this for the time T, I use a 24 h window of 1-min data as:

$$v(t=T) = k\sum_{i=0}^{2}\sum_{j=T-1439}^{T}\left(B_{i,j}-\bar{B}_i\right)^2 \tag{11}$$

where $B_0 = Nr$, $B_1 = Er$, $B_2 = Zr$, k = 1/(3 · 1440) and $\bar{B}_i$ is the mean of the i'th component within the window. I include all three components and $v(t = T)$ is defined from the 24 h of data prior to the actual data point. The logic behind a non-centered window is that the future should not affect the present but the past can. Equation (11) is a summarization of variance for each component and provides a simple measure of disturbance for each minute of the year.

[71] One complication remains. Long duration storms can result in a large $v(t)$ value during the storm main phase but may produce low values during the recovery phase. As a result the daily values as determined by the yearly trend may slightly follow the storm depression (Figure 8). To overcome this problem I introduce a 'memory' of the system by applying a decay to the one minute $v(t)$ parameter from (11). This, is done by summarizing the scaled $v(t)$ from the previous 8 days:

$$d(t=T) = \sum_{j=T-8*1440}^{T-1} f\cdot k\cdot v_j\cdot\left[1+\cos\left[(T-j)\cdot\frac{\pi}{8\cdot 1440}\right]\right] \tag{12}$$

where

$$f = \begin{cases} |\cos(mlat)|, \textit{ for the } N-\textit{component} \\ 0, \textit{ for the } E-\textit{component} \\ |\sin(mlat)|, \textit{ for the } Z-\textit{component} \end{cases}$$

and k = 1/(8 · 1440), *mlat* is the magnetic latitude of the station. The function, *f*, is introduced due to the latitudinal dependence of the ring current as measured by each component. For the E-component $f = 0$, and thus I assume that the delayed ring current effect on the E-component is negligible. The time dependent scaling function was chosen to be a cosine. While this could be another function the cosine fulfills three requirements: (1) continuous function, (2) decrease from unity to zero, and (3) small gradients for times near start and end of window. Likewise, one may argue that the 8 day window is arbitrarily chosen. It is, however, based on a typical duration of a magnetic storm recovery phase. Also, keep in mind that the scaling function (cosine) is selected to have a small gradient near the end of the window and is thus fairly insensitive to minor changes in the window size. For magnetic latitudes above 60 degrees I define d = 0 as the perturbations are primarily due to auroral electrojet activity with decay times on the order of hours and not days.

[72] From the two disturbance values, *v* and *d*, I determine the disturbance level and thereby uncertainty of the data:

$$U = v + d \tag{13}$$

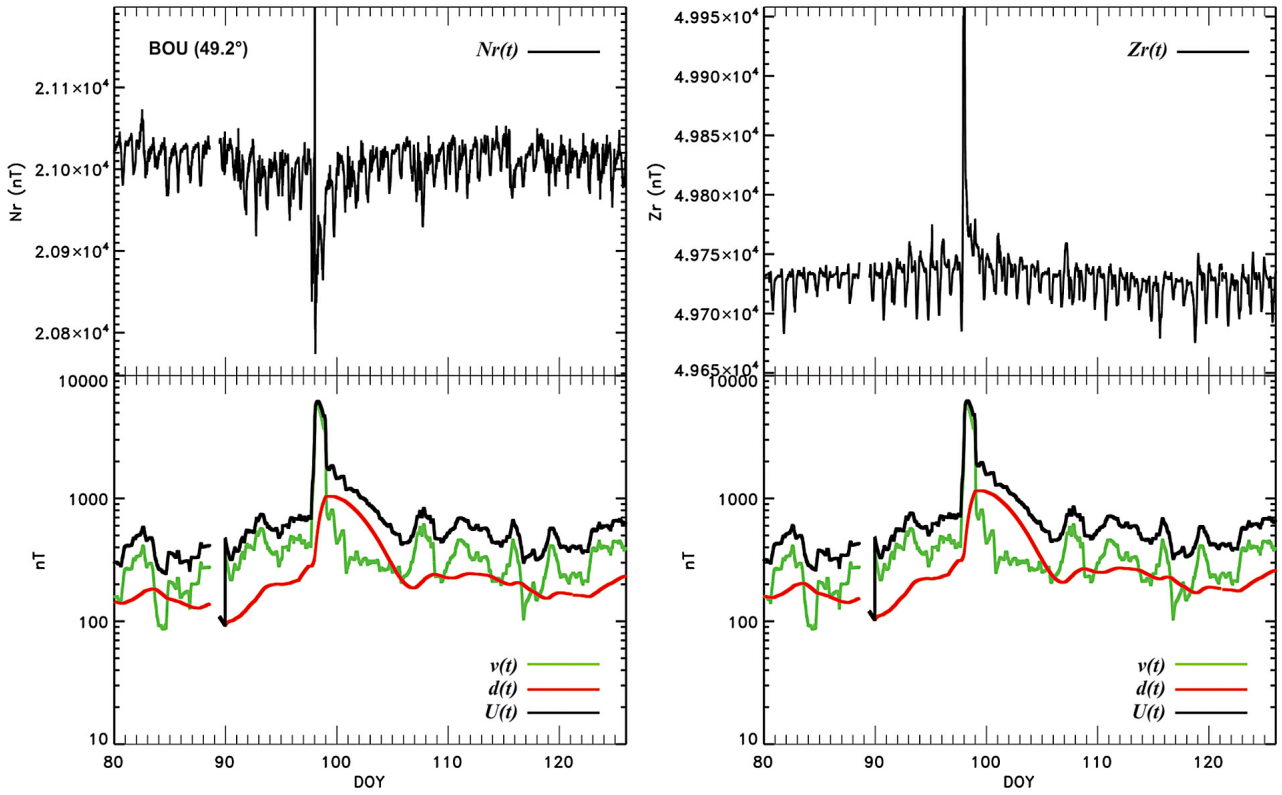

Figure 14. (left) N-component and (right) Z-component. (top) The same 36 day interval (year 2000) shown in Figure 8 but for a midlatitude station. (bottom) The weighting functions, *v*, *d*, and *U* (see text for explanation).

where all parameters are defined above. The variable *v* is the variance and provides only instantaneous information of the spread in the data while *d* can be interpreted as the time delayed effect of the variance and provides information regarding the memory of the system. The value *U* can thus be interpreted as a modified variance. Figure 14 shows *Nr* and *Zr* (Figure 14, top) and the uncertainties, *v*, *d*, and *U* (Figure 14, bottom) for the same period shown in Figure 8 but for a midlatitude station, BOU. The *Er* component is not shown as it shows no long duration ring current effects. The Y-scale is logarithmic and the uncertainty of the data (I can take the square root of *U* and refer to it as the modified standard deviation) around the major storm is more than 2-orders of magnitude greater than during the most quiet periods. For the weighted smoothing used for the final step of the yearly trend, this results in the data not carrying any significant weight and they are thus more or less ignored by the smoothing algorithm. Notice that introducing the decay or 'memory' results in an increase in the uncertainty, *D*, in the storm recovery phase that is not otherwise considered 'noisy' if only the variance, *v*, is used. It is this time history of the uncertainty that was used for the weighted smoothing of the yearly trend thereby removing the slight depression seen in the daily values (Figure 8 red diamonds). If desired one can use the *U* parameter to identify quiet time and disturbed time periods or days.

[73] Thus, each station has its own information regarding disturbance level. The above approach acknowledges the concerns of the *Joselyn* [1989] paper (points 1–3), my four concerns (points 4–7), and finally my third requirement (data handling must be self-contained, see section 2). In my technique there is no need for any so-called quiet days and thus I avoid all the inherent problems associated with their identification.

7.2. Observatories Versus Variometers

[74] While there are many types of ground based magnetometers they can be organized by two general groups: (1) observatories and (2) variometers. The former provides absolute measurements of the field while the latter does not. Variometers can only be used to study variations of the field and thus require the removal of a more or less arbitrary offset. Most often variometers are built and operated on small research budgets while observatories are highly sophisticated instruments built and operated under strict regulations (see for example the INTERMAGNET technical manual, www.intermagnet.org). For those operating variometers it may be of interest to perform the statistical analysis above to answer the question of whether there are fundamental differences in the performance. Thus, I plot the *FWHM* data from Figure 12 but separate the stations into observatories and variometers. As Figure 15 vividly shows I find no systematic differences between the two groups of instruments. This result should not be taken to indicate that the two types provide measurements with the same noise level. Rather I interpret the result as an indication that the differences in noise level are statistically far smaller than the variations of the M-I current system. Thus, the cheaper variometers are sufficient for the purpose

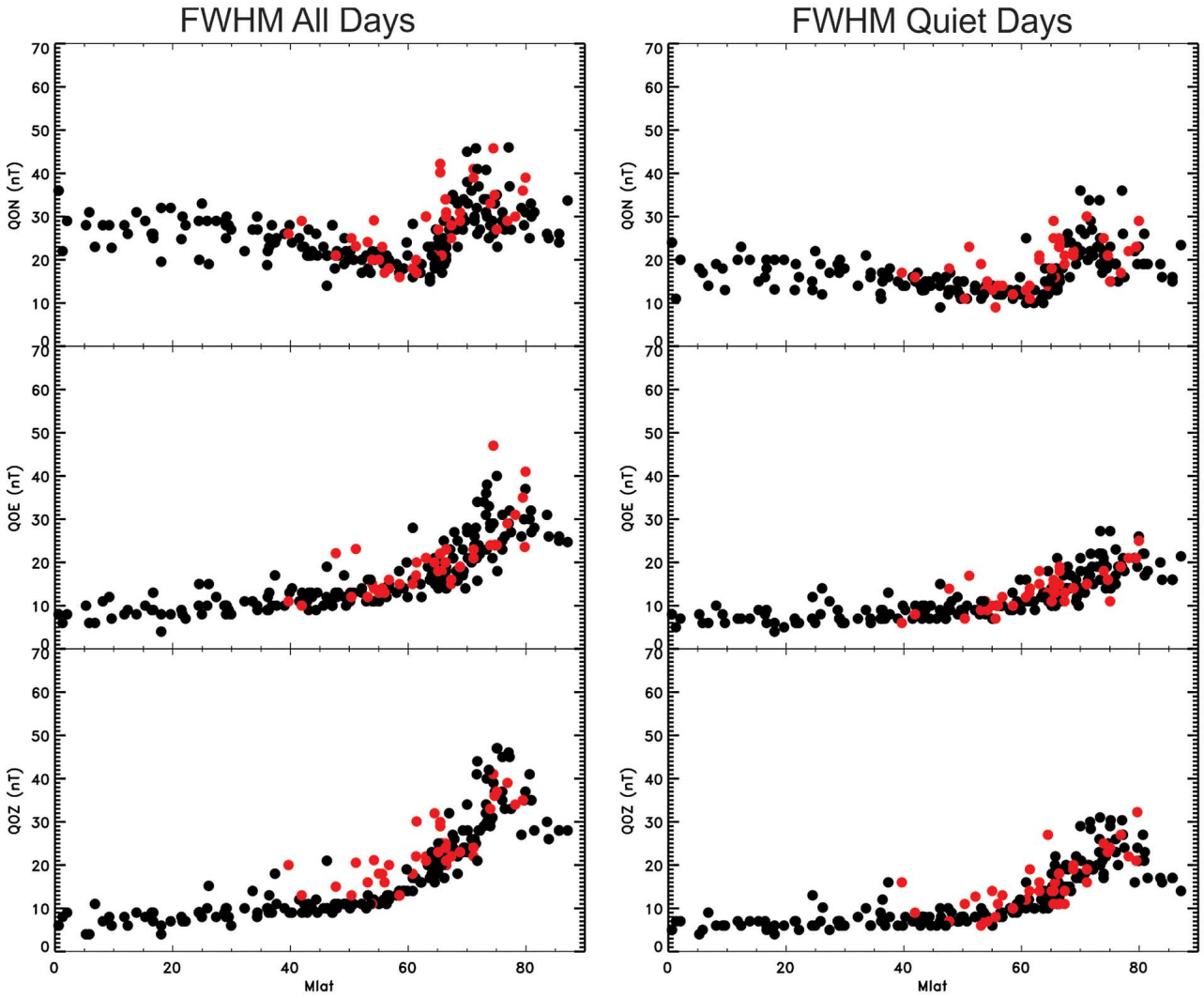

Figure 15. Same format as Figure 12. Black dots are magnetic observatories while red dots are variometer stations.

of studying the M-I current system with a 1-min temporal resolution. This may or may not be the case for higher time resolution data. Also, it makes the assumption that the offsets are either known or small compared to the horizontal X- or H-component (see equation (3)).

8. Summary and Conclusions

[75] In this paper I outlined the data processing technique which is used in the SuperMAG initiative. SuperMAG is a worldwide collaboration of organizations and national agencies that currently operate more than 300 ground based magnetometers. SuperMAG provides easy access to validated ground magnetic field perturbations in the same coordinate system, identical time resolution and with a common baseline removal approach. The purpose of SuperMAG is to help scientists, teachers, students and the general public have easy access to measurements of the Earth's magnetic field. Easy access to data, plots and derived products maximizes the utilization of this unique data set. It was outlined how SuperMAG processes observations obtained by the individual data provider. Data are rotated into a local magnetic coordinate system by determining a time dependent declination angle. This angle was shown to display a slow gradual change and a yearly periodic variation attributed to changes in the Earth main field and season temperature variations. The baseline is determined from the data itself in a three step process: (1) a daily baseline, (2) a yearly trend, and (3) a residual offset. This technique does not require so-called quiet days and thus it avoids all the well-known problems associated with their identification. The residual offset for the N- and Z-components shows a distinct latitudinal dependence while the E-component is independent on the latitude. This result was interpreted as being due to a weak ring current (likely asymmetric) which is present even during official quiet days. For the purpose of M-I research using 1-min data I find no difference between observatories and variometers. I finally argue that there is no correct baseline determination technique since we do not have a set of ground-truth observations required to make an objective evaluation. Instead, the

user must keep in mind the assumptions on which the baseline was determined and draw conclusions accordingly.

[76] **Acknowledgments.** I would like to thank S. Ohtani and B. Carlson for helpful and constructive comments. For the ground magnetometer data I acknowledge: Intermagnet; USGS, Jeffrey J. Love; Danish Meteorological Institute; CARISMA, PI Ian Mann; CANMOS; The S-RAMP Database, PI K. Yumoto and K. Shiokawa; The SPIDR database; AARI, PI Oleg Troshichev; The MACCS program, PI M. Engebretson, Geomagnetism Unit of the Geological Survey of Canada; GIMA; MEASURE, UCLA IGPP and Florida Institute of Technology; SAMBA, PI Eftyhia Zesta; 210 Chain, PI K. Yumoto; SAMNET, PI Farideh Honary; The institutes who maintain the IMAGE magnetometer array, PI Eija Tanskanen; PENGUIN; AUTUMN, PI Martin Conners; Greenland magnetometers operated by DTU Space; South Pole and McMurdo Magnetometer, PI's Louis J. Lanzerotti and Alan T. Weatherwax; ICESTAR; RAPIDMAG; PENGUIn; British Antarctic Survey; BGS, PI Dr. Susan Macmillan; IZMIRAN, Vladimir Kuznetsov and Valery Petrov.

[77] Robert Lysak thanks the reviewers for their assistance in evaluating this paper.

References

Anderson, B. J., M. J. Engebretson, S. P. Rounds, L. J. Zanetti, and T. A. Potemra (1990), A statistical study of Pc3–5 pulsations observed by the AMPTE/CCE magnetic field experiment: 1. Occurrence distributions, *J. Geophys. Res.*, *95*(A7), 10,495–10,523, doi:10.1029/JA095iA07p10495.

Elkington, S. R., M. K. Hudson, and A. A. Chan (1999), Acceleration of relativistic electrons via drift-resonant interaction with toroidal-mode Pc-5 ULF oscillations, *Geophys. Res. Lett.*, *26*(21), 3273–3276, doi:10.1029/1999GL003659.

Friis-Christensen, E., M. A. McHenry, C. R. Clauer, and S. Vennerstrom (1988), Ionospheric traveling convection vortices observed near the polar cleft: A triggered response to changes in the solar wind, *Geophys. Res. Lett.*, *15*, 253–256, doi:10.1029/GL015i003p00253.

Gjerloev, J. W. (2009), A global ground-based magnetometer initiative, *Eos Trans. AGU*, *90*(27), 230–231, doi:10.1029/2009EO270002.

Gjerloev, J. W., R. A. Hoffman, S. Ohtani, J. Weygand, and R. Barnes (2010), Response of the auroral electrojet indices to abrupt southward IMF turnings, *Ann. Geophys.*, *28*, 1167–1182, doi:10.5194/angeo-28-1167-2010.

Gjerloev, J. W., S. Ohtani, T. Iijima, B. Anderson, J. Slavin, and G. Le (2011), Characteristics of the terrestrial field-aligned current system, *Ann. Geophys.*, *29*, 1713–1729, doi:10.5194/angeo-29-1713-2011.

Glassmeier, K. H., M. Honisch, and J. Untiedt (1989), Ground-based and satellite observations of traveling magnetospheric convection twin vortices, *J. Geophys. Res.*, *94*, 2520–2528, doi:10.1029/JA094iA03p02520.

Janzhura, A. S., and O. A. Troshichev (2008), Determination of the running daily geomagnetic variation, *J. Atmos. Sol. Terr. Phys.*, *70*, 962–972, doi:10.1016/j.jastp.2007.11.004.

Joselyn, J. A. (1989), Geomagnetic quiet day selection, *Pure Appl. Geophys.*, *131*(3), 333–341, doi:10.1007/BF00876832.

Kamide, Y., and S. Kokubun (1996), Two-component auroral electrojet: Importance for substorm studies, *J. Geophys. Res.*, *101*, 13,027–13,046.

Kihn, E. A., and A. J. Ridley (2005), A statistical analysis of the assimilative mapping of ionospheric electrodynamics auroral specification, *J. Geophys. Res.*, *110*, A07305, doi:10.1029/2003JA010371.

Lanzerotti, L. J., L. C. Lee, C. G. Maclennan, A. Wolfe, and L. V. Medford (1986), Possible evidence of flux transfer events in the polar ionosphere, *Geophys. Res. Lett.*, *13*, 1089–1092, doi:10.1029/GL013i011p01089.

Lu, G., et al. (1996), High-latitude ionosphere electrodynamics as determined by the assimilative mapping of ionospheric electrodynamics procedure for the conjunctive SUNDIAL/ATLAS 1/GEM period of March 28–29, 1992, *J. Geophys. Res.*, *101*, 26,697–26,718, doi:10.1029/96JA00513.

Mayaud, P. N. (1980), *Derivation, Meaning, and Use of Geomagnetic Indices*, *Geophys. Monogr. Ser.*, vol. 22, 154 pp., AGU, Washington, D. C., doi:10.1029/GM022.

McPherron, R. L. (1970), Growth phase of magnetospheric substorms, *J. Geophys. Res.*, *75*, 5592–5599, doi:10.1029/JA075i028p05592.

Menvielle, M., N. Papitashvili, L. Hakkinen, and C. Suckdorff (1995), Computer production of K indices: Review and comparison of methods, *Geophys. J. Int.*, *123*, 866–886.

Murr, D. L., and W. J. Hughes (2001), Reconfiguration timescales of ionospheric convection, *Geophys. Res. Lett.*, *28*, 2145–2148, doi:10.1029/2000GL012765.

Newell, P. T., and J. W. Gjerloev (2011a), Evaluation of SuperMAG auroral electrojet indices as indicators of substorms and auroral power, *J. Geophys. Res.*, *116*, A12211, doi:10.1029/2011JA016779.

Newell, P. T., and J. W. Gjerloev (2011b), Substorm and magnetosphere characteristic scales inferred from the SuperMAG auroral electrojet indices, *J. Geophys. Res.*, *116*, A12232, doi:10.1029/2011JA016936.

Newell, P. T., and J. W. Gjerloev (2012), SuperMAG-based partial ring current indices, *J. Geophys. Res.*, *117*, A05215, doi:10.1029/2012JA017586.

Nishida, A. (1971), DP 2 and polar substorms, *Planet. Space. Sci.*, *19*, 205–221.

Park, S., and R. Schowengerdt (1983), Image reconstruction by parametric cubic convolution, *Comput. Vision Graphics Image Processing*, *23*, 258–272.

Richmond, A. D., and Y. Kamide (1988), Mapping electrodynamic features of the high-latitude ionosphere from localized observations: Technique, *J. Geophys. Res.*, *93*, 5741–5749, doi:10.1029/JA093iA06p05741.

Ridley, A. J., and E. A. Kihn (2004), Polar cap index comparisons with AMIE cross polar cap potential, electric field, and polar cap area, *Geophys. Res. Lett.*, *31*, L07801, doi:10.1029/2003GL019113.

Soraas, F., and L. R. Davis (1968), Temporal variations of the 100 keV to 1700 keV trapped protons observed on satellite Explorer 26 during first half of 1965, *NASA Tech. Memo.*, *TM-X-612-68-328*, 52 pp.

Takahashi, K., and B. J. Anderson (1992), Distribution of ULF energy ($f < 80$ mHz) in the inner magnetosphere: A statistical analysis of AMPTE CCE magnetic field data, *J. Geophys. Res.*, *97*(A7), 10,751–10,773, doi:10.1029/92JA00328.

Takahashi, K., B. Toth, and J. V. Olson (2001), An automated procedure for near-real-time Kp estimates, *J. Geophys. Res.*, *106*, 21,017–21,032, doi:10.1029/2000JA000218.